Nuclear Materials and Energy 15 (2018) 220–225

Contents lists available at ScienceDirect

Nuclear Materials and Energy

journal homepage: www.elsevier.com/locate/nme

WCrY smart alloys as advanced plasma-facing materials – Exposure to steady-state pure deuterium plasmas in PSI-2

J. Schmitz[*,a,b], A. Litnovsky[a], F. Klein[a], T. Wegener[a], X.Y. Tan[a,d], M. Rasinski[a], A. Mutzke[c], P. Hansen[a], A. Kreter[a], A. Pospieszczyk[a], S. Möller[a], J.W. Coenen[a], Ch. Linsmeier[a], U. Breuer[e], J. Gonzalez-Julian[a], M. Bram[a]

[a] Forschungszentrum Jülich GmbH, Institut für Energie- und Klimaforschung, Jülich, 52425, Germany
[b] Department of Applied Physics, Ghent University, Ghent, 9000, Belgium
[c] Max-Planck-Institute for Plasmaphysics, Wendelsteinstrasse 1, Greifswald, 17491, Germany
[d] School of Materials Science and Engineering, Hefei University of Technology, Hefei, 230009, China
[e] Forschungszentrum Jülich GmbH, Zentralinstitut für Engineering, Elektronik und Analytik, Jülich, 52425, Germany

ARTICLE INFO

Keywords:
Smart alloys
Plasma-wall-interaction
Plasma ion irradiation
DEMO
W-based alloys

ABSTRACT

In this paper the impact of steady state pure D plasma on WCrY smart alloys at ion energies of 120 and 220 eV is reported. For this purpose a comparison with simultaneously exposed pure W samples is drawn. Different analysis techniques employed for pre- and post-plasma sample analysis hint at a significant depletion of Cr and enrichment of W for lower ion energies. Preferential sputtering leads to enhanced volumetric loss at 220 eV. Analysis of redeposited material indicated local redeposition of Cr. Modelling the ion irradiation with SDTrimSP is used to further interpret experimental results. Depending on the sample temperature during plasma exposure and the magnitude of the ion flux, diffusion of Cr towards the surface is a determining factor for erosion of smart alloys for higher ion energies.

1. Introduction

An essential part of future fusion reactors is the so-called first wall, the wall directly facing the plasma and therefore protecting structural parts of the vessel. Only a few materials are suitable to be used in fusion environment. Among other requirements described for instance in [1], the armour material has to withstand high heat loads, feature low tritium retention and moreover show only minor activation during neutron irradiation. Tungsten (W), currently the preferred first wall material for the next step fusion devices such as DEMO, possesses many advantages. These include a very high melting point and low erosion yields during ion irradiation. However, for the development of W-based wall components some of the material's drawbacks have to be improved. Besides its inherent brittleness, a further drawback of pure W consists in fast oxidation when coming into contact with oxygen (O). During accidental reactor conditions (Loss-Of-Coolant-Accident: LOCA) the cooling system fails. Additionally air ingress may occur. W oxidises and forms radioactive WO_3. Due to nuclear decay heat wall temperatures rise to above 1000°C for several months [2] leading to the mobilisation of radioactive material into the environment. In order to establish intrinsic reactor safety, W-based smart alloys are currently being developed aiming at preserving W-like behaviour during plasma operation while suppressing oxidation in case of LOCA. The most promising systems in terms of passivation behaviour feature chromium (Cr) as passivating element as well as yttrium (Y) [3]. Y serves as active element facilitating Cr transport towards the alloy's surface during oxidation and adding to the stability of the oxide scale. So that according to [4] the addition of Y to the WCr-system reduces the mass gain significantly by supporting the formation of a continuously growing, well adhering and dense Cr_2O_3 layer. These alloying elements possess a lighter mass compared to W and are therefore more easily sputtered during plasma operation. Preferential sputtering leads to depletion of Cr and Y, and enrichment of W, leaving a pure W surface facing the plasma.

Newly developed WCrY-systems demonstrated a significant oxidation suppression of more than five orders of magnitude in comparison to pure W [5]. In 2017 these systems have been exposed to plasma for the first time [5]. This paper reports in detail on the first plasma exposure of WCrY smart alloys. Moreover experimental findings of a recently conducted second plasma experiment at lower ion energies are covered and a comparison to simulation results obtained with SDTrimSP [6] are drawn.

* Corresponding author.
E-mail address: jan.schmitz@fz-juelich.de (J. Schmitz).

https://doi.org/10.1016/j.nme.2018.05.002
Received 28 November 2017; Received in revised form 13 April 2018; Accepted 8 May 2018
Available online 16 May 2018

2. Experimental setup and analytic techniques

2.1. Sample preparation

Samples used for the plasma experiments reported in this paper were obtained by using Field-Assisted Sintering Technology (FAST) [7] at Forschungszentrum Jülich (FZJ). The composition of all exposed smart alloy samples is W-11.4wt%Cr-0.6wt%Y. WCrY samples exposed simultaneously were produced from the same powder batch. The name convention is as follows: samples SA11 and SA12 were exposed during the first plasma experiment (PE1) at an ion energy of 220 eV, while samples SA21 to 23 were exposed during the second experiment (PE2) at lower ion energies (120 eV). For the sintering process of samples SA11 and SA12 a uniaxial ramp of 200 °C/min, a maximum pressure of 50 MPa and a holding time of 1 min at a maximum temperature of 1550 °C were used. FAST parameters for samples SA21 to SA23 differ from SA11 and SA12 in a maximum temperature of 1460 °C after which no holding time was applied.

The WCrY samples investigated in the two plasma exposures were produced using slightly different FAST parameters. For samples in the second plasma experiment, SA21 to SA23, optimised FAST parameters were used. As a result for these samples a fine sub-micrograin structure and improved oxidation resistance as referred in [5] compared to samples produced for the first plasma experiment were obtained. However, plasma performance is not expected to significantly differ. There may be a small difference due to enhanced Cr-mobility by providing smaller grains and thus more grain boundaries in the material. Consequently, bulk WCrY samples with small WCr-grains and finely dispersed yttrium oxide (Y_2O_3) particles were obtained. Because of the small size of the yttrium oxide particles it is difficult to investigate the exact composition of the yttrium oxide, but as Y_2O_3 is the most stable yttrium oxide we assume most of the yttrium oxide to have this stoichiometry. Details of the sample production and the resulting microstructure can be found in [5].

Samples are cut from the smart alloy ingots by means of wire erosion to fit the PSI-2 mask geometry. To be able to hang the samples in the furnace for oxidation studies after exposure, a hole is added to the sample geometry (see Fig. 2c). W samples exposed alongside with the afore-mentioned WCrY samples for direct comparison were all cut from the same pure W piece by wire erosion. The plasma-facing surface of W and WCrY samples spans over 1 cm × 1 cm. In order to remove residues from the wire erosion process and ensure the same surface properties, all samples were manually ground. For this purpose different silicon carbide grinding papers (SiC P) were used following a defined sequence. The last paper used within this sequence defines the surface roughness of the ground samples. Generally SiC P1200, with a SiC particle size of around 15 µm, is used as the last paper in this sequence. For one W sample and one WCrY sample of PE2, P180 with a SiC particle size of about 82 µm was used to obtain a rougher surface and compare the performance of these samples to the smoother ones.

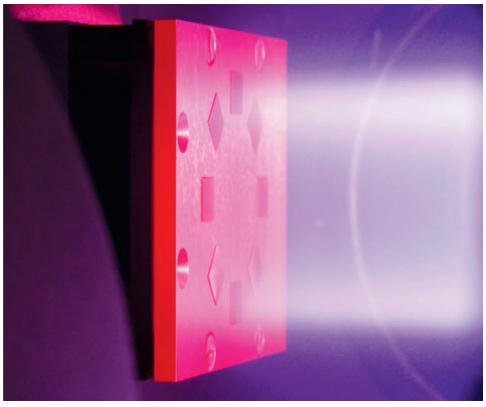

Fig. 1. Plasma exposure of WCrY and W samples in PSI-2.

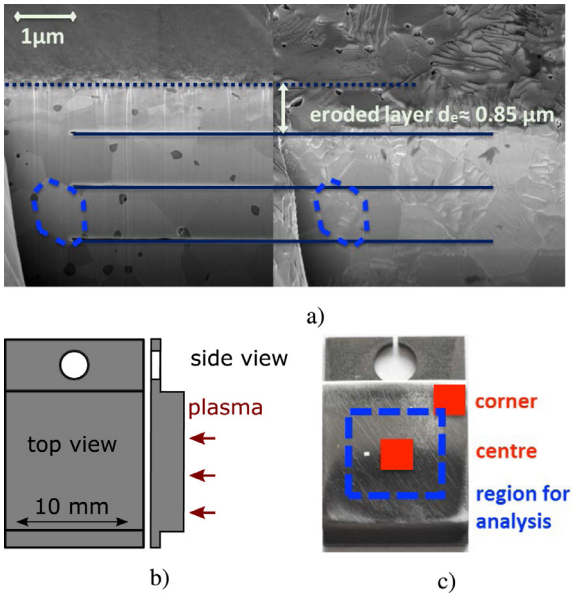

Fig. 2. a) comparison of FIB marker positions relative to the surface before and after plasma for sample SA21, b) sketch of sample geometry for smart alloys, top and side view where the plasma-facing surface is indicated c) photograph of smart alloy (top view), centre and corner positions for FIB craters and analysis region are indicated.

2.2. Analysis methods

A variety of methods were employed for pre- and post-plasma analysis: For assuring a clean sample surface and investigating changes in the smart alloy's depth-resolved composition, Time-of-Flight Secondary Ion Mass Spectroscopy (ToF-SIMS) was used, here the specific setup is IonTof IV. The SIMS technique uses two alternating ion beams for destructive surface analysis. The primary or sputtering ion beam consisted of O^{2+} ions, while Bi^{3+} was used for the analysis presented in this paper. The sputtered area amounts to 300 × 300 µm^2, while the size of the analysed area is 47 × 47 µm^2.

To infer the local erosion during plasma exposure, a crater featuring an orthogonal cut relative to the sample's surface was created by aid of the Focussed-Ion-Beam (FIB) technique prior to plasma exposure. Equidistant markers are generated onto that orthogonal cut (see Fig. 2) so that after plasma exposure the local erosion can be inferred directly by comparing the distance from the surface to the uppermost FIB marker. Within the same analysis device, a combined SEM-FIB system Carl Zeiss CrossBeam XB540, images displaying the sample's surface and microstructure are taken using Scanning Electron Microscopy (SEM). Global erosion or weight loss measurements consist in weighing the samples before and after plasma exposure with a Sartorius MSA225P microbalance with a resolution of 10 µg. With a stylus profiler Dektak 6M several line scans across the sample's surface were conducted, aiming at assessing the surface roughness before and after exposure. During each line scan a tip with a radius of 2.5 µm is drawn across the surface. Linear fitting and discrete fourier transformation are applied for separating defects from cutting or the nonplanarity of the surface from the surface profile before the arithmetic average height R_a (see [8]) is calculated. X-ray Photoelectron Spectroscopy (XPS) is employed to obtain a higher resolution of the elemental composition of the smart alloy's surface composition. For the current XPS-setup, which uses a Al K_α X-ray source, the depth from which radiation is still emitted amounts to approximately 5 nm in W according to the Lambert-Beer law.

At FZJ Nuclear Reaction Analysis (NRA) is available. A μ-NRA setup

with a 4.5 MeV ^3He ion beam was used to detect deuterium (D) retention of the smart alloys. Analysis depth is about 8 μm. Alongside with the NRA detector, Rutherford Backscattering Spectrometry (RBS) is used for analysis of the subsurface elemental sample composition.

2.3. Setup and realisation of experiments

Plasma exposure of the smart alloy samples takes place in the linear plasma device PSI-2 [9] at FZJ. Exposure parameters are based on estimations for conditions at the DEMO first wall [10]. Conditions were chosen on the one hand to resemble conditions of the first plasma exposure of W–Cr–titanium(Ti) smart alloys [11] and on the other hand to facilitate analysis. The WCrY smart alloy samples were exposed alongside with pure W samples for direct comparison. Up to eight samples can be placed simultaneously onto the target holder. Samples are placed symmetrically at the same radial position around the plasma z-axis, so that plasma conditions at all the samples are comparable. For both plasma experiments steady-state pure D plasma was used. In PSI-2 plasmas the oxygen fraction typically amounts to a few 0.1 %. Sputter thresholds for D on W and Cr are according to [12] around 230 eV and 35 eV, respectively. For O on W the threshold is with a value of 44 eV [12] considerably lower than for D. As a consequence of the subjacent threshold for O sputtering, the minute oxygen content is non-negligible for the material's erosion, especially if the ion energy is below the threshold of the main plasma component. The plasma temperature was 6 to 8 eV, further parameters can be found in Table 1. The mask containing the samples is mounted on top of a water-cooled target holder. To warrant good thermal contact between the cooling and the samples a thermal contact material is placed between the back of the samples and the sample holder. For PE1 a layered structure of graphite foil on top of a small Cu spacer with again graphite foil at the rear side of the Cu spacers was used for this purpose. As some of the samples were slightly sticking to the formidable graphite foil after exposure, it was decided to omit the graphite foil layer adjacent to the samples' backside for PE2.

For one sample in PE2, W24, Magnetron-Sputtering was used to coat half of the pure W sample with a WCrY layer of about 4 μm thickness. The composition of this layer is about W-10wt%Cr-1wt%Y. Due to having a pure W layer directly by the side of a WCrY layer, it is possible to study Cr sputtering and redeposition in more detail. Possible Cr redeposition can be detected on the previously clean W surface. For this purpose several Energy-dispersive X-ray Spectroscopy (EDX) spectra were acquired with the combined SEM-FIB system before and after plasma exposure. These spectra allow to identify present elements on a material's surface.

Once the plasma is started, the manipulator with the sample holder at its extreme end is placed in the axially symmetric cylindrical plasma of PSI-2. During exposure plasma parameters such as temperature or ion flux are monitored by means of a retractable Langmuir Probe. The bias voltage is applied between sample holder and machine ground, the ion energy results from the difference of bias voltage and plasma potential. For measuring the sample temperature a thermocouple within the target holder is used. Additionally for PE2, an infrared-camera was employed to monitor the temperature of each sample individually. Moreover, several spectroscopy measurements aiming at detecting Cr and W line radiation were conducted during PE2.

Table 1
Experimental plasma parameters in PSI-2.

	Ion energy [eV]	Ion flux [ions/m^{2}s]	Ion fluence [ions/m^2]	Sample temperature [°C]
PE1	220	5.5×10^{21}	1×10^{26}	620–650
PE2	120	2.7×10^{21}	1×10^{26}	620–700

3. Experimental results and interpretation

3.1. PE1

Comparing the weight loss of pure W and smart alloy WCrY samples it was found that all samples lost around 1100 to 1300 μg of their initial mass during plasma exposure. In contrast to this, the volumetric loss is nearly a factor two greater for the smart alloys compared to W. The lighter alloying elements are sputtered more easily than the heavy element W and contribute (due to their lighter mass) to the higher volumetric loss at nearly the same weight loss as pure W. Weight and volumetric loss (FIB-measured eroded layer thickness d_e), as well as roughness R_a values are displayed in Table 2. Additionally, the calculated eroded layer thickness d_e, based on the global weight loss, is shown and agrees within error bars with measured values. As a conclusion one can say that the plasma erosion of the samples is homogeneous across the samples' surface. This is supported by the fact that the FIB measurements at the centre (SA11) and at one corner (SA11c) of SA11 are consistent. Roughness of the samples is predominantly determined by the grinding paper used in the last step of the sample preparation procedure. Hence the surface roughness amounts to approximately 30 nm for all samples. After plasma exposure all samples showed a slight increase in surface roughness. Due to erosion and redeposition of sputtered material the surface is gradually roughened, still at the relatively low ion energy of 220 eV no major destruction of the surface is to be expected. In Fig. 3 the relative change of elemental composition of SA11 along its depth is shown. The intensities of the W-, Cr- and Y-signals are normalised to be one at the deepest data point of the SIMS analysis. Here we assume that the initial elemental properties of the bulk material is reached, thus the relative change of elemental composition towards the surface (depth = 0 nm) is displayed. All three signals show a constant behaviour in the first graph, i.e. before plasma exposure. Y shows an increase starting from about 20 to 30 nm below the surface. This behaviour can be attributed to the accumulation of yttrium oxide particles in the subsurface layer (see Fig. 4a), which is damaged by manual grinding and agrees well with the particle size of the yttria. In Fig. 4b the small black holes on the plasma-exposed surface are suspected to correspond to locations of sputtered Y_2O_3 particles. This conclusion is drawn from the smart alloys' microstructure, where the yttrium oxide particles are dispersed in between WCr-grains and further from the surface analysis: for the post-plasma SIMS analysis of SA11 the Y-signal diminishes closer to the surface whereas W- and Cr-signals do not show significant deviation from the pre-plasma elemental composition. From this comparison a clear depletion of only Y, not Cr and hence no clear enrichment of W towards the surface is inferable. To look more closely at the plasma impact onto the surface composition, XPS-analysis was performed on an unexposed piece of SA11, as well as on the plasma-exposed SA12. In Table 3 one can see that for the non-exposed sample, even without Ar-cleaning, Cr and Y are, besides W, clearly present. When doing the same analysis on the plasma-exposed sample SA21, one cannot find any Cr or Y without Ar-treatment. Even after Ar-cleaning and hence removal of the very top surface layer no Y is visible. The findings for SA21e and SA21ec as shown in the table support the Y depletion towards the surface. In addition they imply the existence of a thin near-surface layer of approximately 3 nm thickness where W is enriched and Cr depleted. Amplification of the Y-signal for XPS of SA11 compared to sample composition from production parameters (see Section 2) can be ascribed to a more intensive contribution of elements at the very surface of the XPS-analysed layer.

NRA results for D retention in WCrY are within expectations for the relatively high sample temperatures of around 650 °C. An amount of about $(1.0 \pm 0.1) \cdot 10^{14}$ at /cm^2 was measured for the first 3 μm below the surface and $(2.0 \pm 0.2) \cdot 10^{14}$ at /cm^2 below 3 μm up to a depth of 8 μm. These detected values agree with available data from similar experiments for W [13]. For determining the plasma impact on the

Table 2
Weight loss and roughness before and after plasma in PE1.

	weight loss [μg]	$R_{a\,[nm]}$ before	R_a[nm] after	d_e [μm] measured	d_e [μm] calculated
W11	1200 ± 10	41 ± 6	47 ± 6	0.46 ± 0.11	0.62 ± 0.10
W12	1093 ± 10	28 ± 4	33 ± 5	0.44 ± 0.22	0.56 ± 0.10
SA11	1223 ± 10	30 ± 4	34 ± 7	0.84 ± 0.17	0.77 ± 0.13
SA11c	1223 ± 10	30 ± 4	34 ± 7	0.90 ± 0.21	0.77 ± 0.13
SA12	1287 ± 10	24 ± 5	25 ± 4	0.87 ± 0.22	0.80 ± 0.13

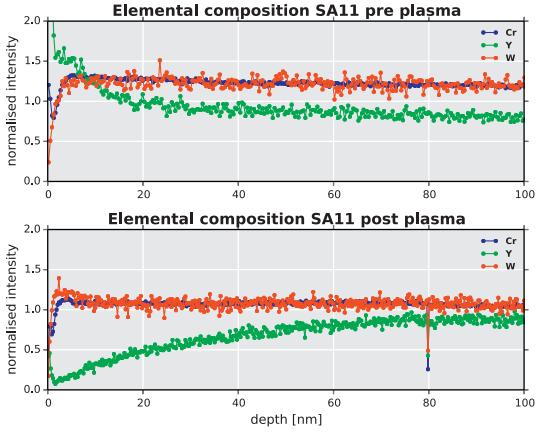

Fig. 3. SIMS-analysis for W, Cr and Y in PE1.

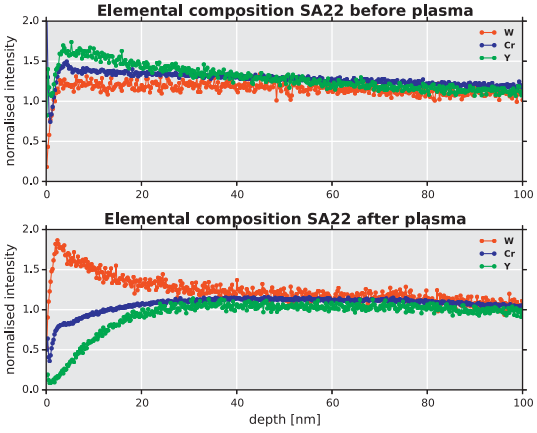

Fig. 5. SIMS-analysis for W, Cr and Y in PE2.

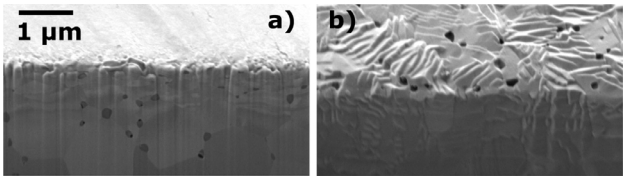

Fig. 4. SEM picture of upper edge of FIB cut for SA11 before (a) and after plasma exposure (b).

Table 3
Percental fraction [%] of elements detected by XPS, e: exposed, ec: exposed and cleaned by Argon ions. Error by manual peak-fitting is of the order of 10 % of obtained results.

	% W	% Cr	% Y
SA11	79	17	4
SA21e	100	0	0
SA21ec	88	12	0

smart alloy's oxidation behaviour, oxidation of a plasma-exposed sample has been performed and compared to a non-exposed sample. Results are presented in [5]. Oxidation performance of the two above-mentioned samples deviates slightly, yet this may be a result of plasma impact as well as of marginally different geometries. As surface roughness is a detrimental factor for the oxidation performance and not all edges of the plasma-exposed samples are ground due to the geometry, the second possibility is more likely.

3.2. PE2

The main difference between the two experiments PE1 and PE2 is the ion energy owing to biasing the target. Results for the plasma exposure at 120 eV, PE2, are described in this section. As a consequence of the direct contact under high pressure and high temperatures of the Cu blocks and the W/WCrY samples, all but two samples could not be disconnected from the Cu anymore, which is why measuring the weight loss due to plasma erosion was not possible.

For PE2 depletion of Y and Cr is clearly visible in the SIMS-profiles (see Fig. 5). At the same time the W signal increases considerably towards the surface. As an ion energy of 120 eV is clearly below the sputter threshold for D ions on W, W is enriched at the surface. This finding is reflected in the local erosion values obtained from FIB, displayed in Table 4. Although for the WCrY samples d_e is slightly higher, a nearly identical volumetric loss is indicative of W enrichment towards the surface for the smart alloys. Initially, when plasma operation starts, the alloying elements are depleted while W remains on the surface. As this heavy element now determines superiorly the erosion yield, the WCrY yield becomes comparable to that of pure W. Sputtering during these experiments is believed to originate mainly from small amounts of O ions in the plasma (see Section 4). The EDX-spectra on the WCrY-coated and uncoated W sample (see Fig. 6) are indicative of Cr-redeposition next to the coating edge. At the same time, Cr-content on the surface of the WCrY-coating decreased during plasma operation (see spectrum 1). Hence sputtered Cr was only observed to redeposit locally rather than globally. For spectroscopy measurements during plasma operation neither W- nor Cr-line radiation was visible in the spectra. Too few particles of both W and Cr were sputtered so that signals were below the detection limit.

The surface roughness evolution of samples exposed in PE2 is similar to the one in PE1. According to Dektak-measured values in Table 4 R_a is marginally incremented, also for rougher samples. From Fig. 7a no distinct agglomeration of Y_2O_3 particles in the subsurface

Table 4
Local erosion and surface roughness in PE2.

	Weight loss [μg]	R_a [nm] before	R_a[nm] after	d_e [μm] measured
W21	na	532 ± 60	584 ± 36	0.17 ± 0.05
W22	na	26 ± 2	30 ± 2	0.18 ± 0.05
W23	na	32 ± 3	28 ± 3	0.21 ± 0.05
W24	na	28 ± 4	28 ± 2	0.18 ± 0.06
SA21	na	43 ± 7	61 ± 19	0.23 ± 0.05
SA22	na	32 ± 5	32 ± 5	0.21 ± 0.05
SA23	na	306 ± 33	319 ± 15	0.21 ± 0.05

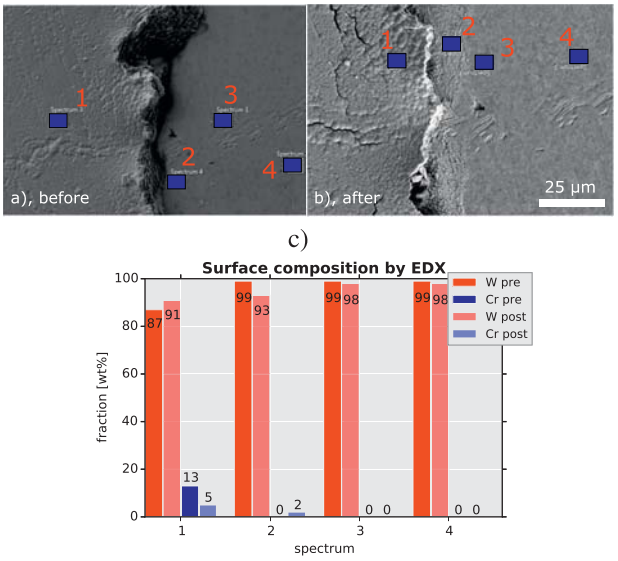

Fig. 6. EDX spectra on coated W24 sample a) before and b) after plasma. Left side of sample with spectrum 1: deposited WCrY, c): EDX spectra 1–4: surface composition of W and Cr in wt%, not displayed O- and C-content add up to 100 wt%.

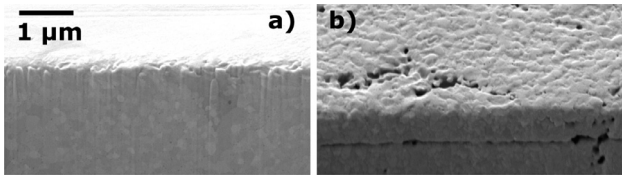

Fig. 7. SEM picture of upper edge of FIB cut for SA22 before (a) and after plasma exposure (b).

layer is observed, which explains the less pronounced increase of the Y-signal in Fig. 5 compared to Fig. 3. Besides, in Fig. 7b one can see not only small black holes owing to sputtered Y_2O_3 particles but also enlarged crater-like holes presumably resulting from Cr depletion. These holes are also visible onto the plasma-exposed orthogonal surface of the FIB cut. Additionally, the FIB generated horizontal markers are still visible after plasma exposure so that the local erosion can be inferred easily. Grain size of SA22 is reduced as against SA11 as a result of different FAST parameters during sample production. Generally the grain size of all samples reported varies slightly as a consequence of the ongoing optimisation of bulk sample production. Still the characteristic microstructure of WCr-grains with finely distributed yttrium oxide particles is preserved.

Similar to D retention for PE1, values obtained for samples exposed in PE2 are within estimates. In the first 3 µm below the surface D retention of W is about $(0.40 \pm 0.04)\cdot 10^{14}$ at /cm^2, while for WCrY a value of $(1.1 \pm 0.1)\cdot 10^{14}$ at /cm^2 was obtained. For the layer below 3 µm and up to a depth of 8 µm the measured W and WCrY values are $(0.39 \pm 0.04)\cdot 10^{14}$ at /cm^2 and $(2.6 \pm 0.3)\cdot 10^{14}$ at /cm^2, respectively. Hence the retention values for WCrY are less than an order of magnitude increased compared to pure W. RBS provides another means for determining the depletion of alloying elements and the enrichment of W below the surface. With a resolution of 50 nm the surface layer Cr content as quantified by RBS is about 26 at%, compared to 30 at% in the bulk for the plasma-exposed WCrY sample. For a non-exposed sample both values amount to 30 at%. As regarding to the SIMS profiles (see Fig. 5) the depletion of Cr extends to a depth of about 35 to 40 nm, the value obtained by RBS is just an average of the Cr content of a layer slightly thicker than the depletion zone. However, one has to keep in mind that the roughness of the non-polished but ground samples might introduce some uncertainties in SIMS analysis. Nevertheless, analysis by RBS once again confirms depletion of Cr for smart alloys exposed in PE2. Experiments on oxidation performance for samples of PE2 will be conducted in the near future.

4. Modelling of ion irradiation

The Monte-Carlo Code SDTrimSP makes use of the Binary-Collision-Approximation (BCA) to simulate ion irradiation of amorphous targets. The underlying physics are described in [6]. For simulating the plasma impact on the WCrY smart alloys the dynamic version of SDTrimSP was used. Herein a one-dimensional target made up of dynamically thickening or shrinking layers is employed. The initial target composition is converted to atomic per cent (at%), this is the input format needed for the SDTrimSP target setup, and corresponds to 67.9at%W-31.1at%Cr-1at%Y. The ion projectiles subsequently shot into the target create recoils and eventually sputtering of subsurface atomic layers if the surface binding energy is overcome.

Concentration gradients within a material lead to diffusion of elements to counteract the build-up of gradients. This diffusion increases exponentially with respect to temperature but is also dependent on other factors such as the microstructure of the investigated material. The thermal diffusion between adjacent target layers can be included in the model since SDTrimSP 5.07 [14] and was used here for diffusion of Cr in the WCrY-system. For comparing the experimental and modelling results experimental local erosion is taken to be around 450 nm for pure W and 850 nm for WCrY.

In Fig. 8 the target composition of WCrY after plasma exposure without and including diffusion of Cr in WCrY is shown. If diffusion is excluded, composition changes are localised within the first few nm beneath the surface (Fig. 8a). At the first subsurface atomic layer Cr and Y are depleted, while W is enriched. Cr content peaks below this layer as Cr atoms are pushed inside by incoming ions, the local Cr agglomeration leads to a decrease in the W concentration. The behaviour of Y is similar to that of Cr, however, as the Y content within the material is only minor its effects are not extensively discussed. Assuming a plasma composition of 99.77 % D and 0.23 % O, a surface recession of 45 nm is obtained for pure W after a fluence of 1×10^{25} ions/m^2, which corresponds to 1/10 of the total accumulated experimental fluence. W erosion was used for setting the O concentration of the plasma in the simulations. Applying the same conditions and not allowing for Cr diffusion, a surface recession of 56 nm is obtained for WCrY. Determining a mean diffusion coefficient to match modelled surface recession with 10 % of the experimental results yields a value of $D_m = 5 \times 10^{-18}$ m^2/s. This coefficient comprises and does not distinguish between the effects of thermal diffusion and diffusion due to plasma induced concentration gradients. It is only valid for the temperature at which the experiment was conducted. Using this diffusion coefficent the simulation yields a surface recession of 85 nm for WCrY, again at a fluence of 1×10^{25} ions/m^2, 10 % of the experimental fluence. The corresponding depth-resolved target composition is displayed in Fig. 8b. Despite evidencing a sudden increase at the surface boundary the Y concentration is constant along the depth. This peak is a consequence of the creation and movement of recoils near the surface (cf. [15]). The Y increase results in a decrease in the W-signal. Apart from

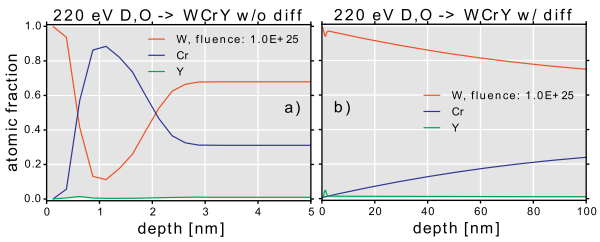

Fig. 8. Simulated WCrY depth-resolved target composition after a fluence of 1×10^{25} D ions/m^2 without (a) and including diffusion (b).

this the W-signal is monotonically increasing towards the surface while Cr decreases, a behaviour reflecting the enrichment of W and depletion of Cr. When allowing for Cr diffusion within the WCrY material, Cr is constantly resupplied towards the surface. This results in the monotonic behaviour of W and Cr signals in Fig. 8b compared to Fig. 8a. As diffusion counteracts the formation of concentration gradients no Cr peak is observed.

5. Comparison of model with experiment (PE1) and discussion

From comparing weight and volumetric loss of the smart alloy samples, it becomes clear that the integration of diffusion is necessary: By dividing the mass loss by the volumetric loss of a WCrY sample, one obtains the theoretical density of the average amount of eroded WCrY during plasma exposure. For PE1 this calculation yields:

$$\rho_e = m_{loss}/V_{loss} \approx 1200\,\mu g/(850\ nm \cdot 1\ cm^2) \approx 14.1\ g/cm^3$$

As ρ_e is smaller than the initial theoretical density of the smart alloy of 15.9 g/cm^3, lighter elements were eroded proportionally more during plasma exposure. An ion energy of 220 eV is about the threshold for physical sputtering of W by D ions (see [12] and [16]). Additionally, the existence of Cr atoms in the vicinity of W atoms beneath the surface leads to enhanced W sputtering. According to BCA the maximum elastic energy transfer between two colliding atoms 1 and 2 is

$$\gamma = 4m_1m_2/(m_1 + m_2)^2$$
$$\gamma_{D,W} \approx 0.04,\ \gamma_{Cr,W} \approx 0.69$$

With an intermediate Cr-W collision instead of the direct energy transfer from D to W the energy transfer factor γ is increased. Thus in the vicinity of Cr atoms W sputtering is augmented. This is another factor contributing to not pronounced enrichment of W in PE1. Besides sputtering by D, the oxygen content of a few 0.1 % for both conducted plasma experiments contributes substantially to the material's erosion. Regarding sputtering by D, different from PE1, in PE2 the D ion energy was well below the threshold for W. At the same time a D ion energy of 120 eV lies above the sputter threshold for D on Cr, which gives rise to a distinctive W enrichment accompanied by Cr depletion as detected by SIMS-analysis (see Fig. 5). Furthermore, this results in a reduced volume loss of WCrY, which is also very similar to that of W (Table 4). The erosion yield was reduced by W enrichment as the sputter yield of pure W is much lower compared to the sputter yield of pure Cr. With mainly W at the surface the overall sputter yield of the alloy is reduced. Another possible reason for less diffusion of Cr in PE2 is the halved ion flux and the resulting decreased rate at which Cr concentration gradients are induced by the plasma.

For reproducing the exact experimental surface composition using SDTrimSP simulations, an extension of the one-dimensional model is required. Generally, experiments and simulations illustrate that the plasma induces changes predominantly in the subsurface target area. However, due to the formation of concentration gradients and diffusion these changes can also affect the samples' bulk material composition.

6. Summary and outlook

This paper reports in detail on the results of the first two plasma exposure experiments (PE1 and PE2) of WCrY smart alloys. Careful sample preparation and pre- and postanalysis is used to investigate the impact of steady-state pure D plasma onto the WCrY and simultaneously exposed W samples. For PE1 experimental and modelling results suggest that Cr diffusion towards the surface is the determining factor for erosion of smart alloys and the reason for a non-significant depletion of Cr and enrichment of W. In contrast to this, at lower ion energies and flux in PE2 preferential sputtering resulting in significant depletion of Cr and Y plus an enrichment of W is clearly visible. As ion energies of around 100 eV are expected for DEMO operation [10], this result and the comparable volume loss of W and WCrY are promising for the application of WCrY smart alloys as first wall material. In PE2 no Cr line radiation originating from the target and expanding into the plasma could be detected, EDX spectra on W4 indicate local redeposition of sputtered Cr. For PE2 oxidation of a plasma-exposed sample still needs to be performed, additionally, SDTrimSP simulations will help interpreting experimental results. We plan to publish a dedicated paper on the inclusion of diffusion into SDTrimSP simulations and comparison with experimental results. The influence of surface topology will be examined in more detail by employing two-dimensional SDTrimSP simulations. As the sputter yield and the induced Cr diffusion may well depend on the ion flux, experiments at higher fluxes and fluences for a more conservative lifetime estimation of the alloys are planned at PSI-2 and other linear plasma devices. Meanwhile the optimisation of bulk sample production at FZJ is ongoing.

Acknowledgements

This work has been carried out within the framework of the EUROfusion Consortium and has received funding from the Euratom research and training programme 2014–2018 under grant agreement No. 633053. The views and opinions expressed herein do not necessarily reflect those of the European Commission.

The research benefited from a grant of the European Commission through the Erasmus Mundus International Doctoral College in Fusion Science and Engineering (FUSION-DC).

References

[1] Ch. Linsmeier, et al., Development of advanced high heat flux and plasma-facing materials, Nucl. Fus. 57 (9) (2017) 092007, http://dx.doi.org/10.1088/1741-4326/aa6f71.
[2] D. Maisonnier, I. Cook, et al., The European power plant conceptual study, Fus. Eng. Des. 75–79 (2005) 1173–1179, http://dx.doi.org/10.1016/j.fusengdes.2005.06.095.
[3] T. Wegener, F. Klein, et al., Development and analyses of self-passivating tungsten alloys for DEMO accidental conditions, Fus. Eng. Des. (2017), http://dx.doi.org/10.1016/j.fusengdes.2017.03.072.
[4] T. Wegener, F. Klein, et al., Development of yttrium-containing self-passivating tungsten alloys for future fusion power plants, Nucl. Mater. Energy 9 (2016) 394–398, http://dx.doi.org/10.1016/j.nme.2016.07.011.
[5] A. Litnovsky, T. Wegener, et al., New oxidation-resistant tungsten alloys for use in the nuclear fusion reactors, Physica Scripta T170 (2017) 014012, http://dx.doi.org/10.1088/1402-4896/aa81f5.
[6] W. Eckstein, Computer Simulation of Ion-Solid Interactions, Springer Series in Materials Science 10 Springer, Berlin and Heidelberg, 1991, http://dx.doi.org/10.1007/978-3-642-73513-4.
[7] O. Guillon, J. Gonzalez-Julian, et al., Field-Assisted sintering technology/spark plasma sintering: mechanisms, materials, and technology developments, Adv. Eng. Mater. 16 (7) (2014) 830–849, http://dx.doi.org/10.1002/adem.201300409.
[8] E.S. Gadelmawla, M.M. Koura, et al., Roughness parameters, J. Mater. Process. Technol. 123 (1) (2002) 133–145, http://dx.doi.org/10.1016/S0924-0136(02)00060-2.
[9] A. Kreter, C. Brandt, et al., Linear plasma device PSI-2 for plasma-material interaction studies, Fus. Sci. Technol. 68 (1) (2015) 8–14, http://dx.doi.org/10.13182/FST14-906.
[10] Y. Igitkhanov, B. Bazylev, et al., The quantification of the key physics parameters for the DEMO fusion power reactor and analysis of the reactor relevant physics issues (KIT Scientific Reports; 7661), doi:10.5445/KSP/1000038935.
[11] A. Litnovsky, T. Wegener, et al., Smart alloys for a future fusion power plant: first studies under stationary plasma load and in accidental conditions, Nucl. Mater. Energy (2016), http://dx.doi.org/10.1016/j.nme.2016.11.015.
[12] W. Eckstein, Sputtered Energy Coefficient and Sputtering Yield, IPP-Report 17/29, (2011).
[13] M.J. Baldwin, R.P. Doerner, et al., Effect of He on D retention in w exposed to low-energy, high-fluence (D, He, Ar) mixture plasmas, Nucl. Fus. 51 (10) (2011) 103021, http://dx.doi.org/10.1088/0029-5515/51/10/103021.
[14] A. Mutzke, R. Schneider, et al., SDTrimSP Version 5.00, IPP-Report 12/8, (2011).
[15] U.v. Toussaint, A. Mutzke, Fluence dependent changes of erosion yields and surface morphology of the iron-tungsten model system: SDTrimSP-2D simulation studies, Nucl. Mater. Energy 12 (2017) 318–322, http://dx.doi.org/10.1016/j.nme.2016.09.005.
[16] K. Sugiyama, K. Schmid, et al., Sputtering of iron, chromium and tungsten by energetic deuterium ion bombardment, Nucl. Mater. Energy 8 (2016) 1–7, http://dx.doi.org/10.1016/j.nme.2016.05.016.